Available online at www.sciencedirect.com
SCIENCE DIRECT®
ELSEVIER
Nuclear Instruments and Methods in Physics Research A 553 (2005) 550–558
NUCLEAR INSTRUMENTS & METHODS IN PHYSICS RESEARCH Section A
www.elsevier.com/locate/nima

Suppression of the slow component of scintillation light in BaF_2

M. Biasini[a,b,*], D.B. Cassidy[a], S.H.M. Deng[a], H.K.M. Tanaka[a,c], A.P. Mills Jr.[a]

[a]*Department of Physics, University of California Riverside, Riverside CA 92521*
[b]*ENEA, Via Don Fiammelli 2, 40129 Bologna, Italy*
[c]*High Energy Accelerator Research Organization, 1-1 Oho, Tsukuba 305-0801, Japan*

Received 14 May 2005; received in revised form 15 July 2005; accepted 15 July 2005
Available online 9 August 2005

Abstract

BaF_2 is a common scintillator material used for the detection of gamma radiation due to its relatively high stopping power, radiation hardness and high luminescence. BaF_2 is often used in gamma ray timing experiments because of the prompt decay component. It is well known that the light output from BaF_2 has two decay components: a prompt one at ~220 nm with a decay constant of around 600 ps and a more intense, temperature dependent, slow component at ~300 nm with a decay constant around 600 ns which hinders fast timing experiments. We report here the development of a gamma ray detector based on a BaF_2 scintillator crystal heated to 220 °C for which the intensity of the slow component is reduced to $(1 \pm 1)\%$. The analysis of the temperature dependent intensity using a model including a single thermally activated quenching mechanism is consistent with the slow component arising from a self-trapped exciton with an activation energy $E = (0.25 \pm 0.01)$ eV.

PACS: 78.55.−m; 29.40.Mc; 29.40.−n; 78.70.Bj

Keywords: Scintillators; Photoluminescence; Positron

1. Introduction

There exist a great many different scintillating materials, with a correspondingly large variation in their properties [1] and in general one chooses a material that is optimum for a particular application. The timing characteristics, in particular, span an enormous range, from a few ns to ms, associated with the emission of photons during electronic transitions in the scintillating material. For the efficient detection of gamma rays for use in positron lifetime experiments [2] an ideal scintillator would be one with a high density and

*Corresponding author.
E-mail address: biasini@physics.ucr.edu (M. Biasini).

0168-9002/$ - see front matter © 2005 Elsevier B.V. All rights reserved.
doi:10.1016/j.nima.2005.07.022

luminosity but a fast decay time [3,4]. However, the general trend is for denser materials to have high luminosities but longer decay times. Table 1 lists some properties of a few commonly used heavy scintillators (all of which are commercially available). We note that recently a ZnO(In) crystal scintillator was shown to have a sub-nanosecond decay time when irradiated with 5.5 MeV alpha particles [5], but is not yet commercially available.

Although the luminosity of BaF_2 relative to, say, NaI(Tl) is rather low it is nevertheless much higher than a usual fast scintillator, such as plastic. Also, the high density of this material ($4.9\,g/cm^3$) makes it well suited for gamma ray detection. Indeed, without the slow component of the scintillation light BaF_2 might be considered as an ideal material for use in positron lifetime experimentation.

It has been demonstrated that the slow light component intensity (and decay time) is temperature dependent [6,7] while the fast component is not. However, it has not previously been shown that the slow component can be fully suppressed by heating. In fact, previous work has largely focused upon cooling crystals to increase the light output of the slow component in order to provide better energy resolution for low energy gamma ray spectroscopy.

The standard method to study scintillation fluorescence decays devised by Bollinger and Thomas [8] employs *a single scintillator* and *two PMs*. Whereas one PM, coupled directly to the scintillator, can be set to trigger on the fast photoelectrons, for the second PM, located a large distance from the scintillator, the probability of detecting single photoelectrons is much less than one. Therefore, by measuring the distribution of the start–stop time intervals, which requires typical times of few hours, the time dependence of the scintillation can be mapped out.

In this work we have used nanosecond bursts of positrons from an accumulator to observe in a single shot the complete fluorescence decay of a BaF_2 scintillator-PM detector as a function of temperature. We find that at $T \simeq 200\,^{\circ}C$ the slow component is essentially completely suppressed while the fast component is unchanged, effectively providing a scintillator with a sub-nanosecond decay time and a *fast* light output of the order of 1000 photons/MeV.

Table 1
Characteristics of some heavy, commercially available scintillators. D is the density in g/cm^3, P is the attenuation length/photoelectric fraction in cm for 511 keV photons, L is the luminosity in photons/MeV for emissions $<10\,\mu s$, $L(0.1)$ is the luminosity in photons/MeV emitted in the first 0.1 ns, $t(50\%)$ and $t(90\%)$ are the time in ns for emission of 50% and 90% of the light, respectively. These data are taken from Ref. [1].

Material	D	P	L	$L(0.1)$	$t(50\%)$	$t(90\%)$
BaF_2	4.89	11.8	12,000	250	320	1340
$Bi_4Ge_3O_{12}$ (BGO)	7.13	2.6	8200	3.7	184	664
$CaWO_4$	6.1	4.7	6000	0.1	4160	13,800
CeF_3	4.11	9.1	4400	22	17	61
CsI(Tl)	4.51	11	64,800	7.5	616	2400
NaI(Tl)	3.67	17	38,000	17	159	530

2. Experimental details

The scintillation properties of BaF_2 were studied using positron bursts containing approximately 5 million positrons obtained from a positron accumulator. This type of accumulator has been described elsewhere [9] and we shall give only a brief overview here. Fig. 1 shows the layout of the accumulator system. Positrons from a 20 mCi ^{22}Na source were moderated using a solid neon moderator to produce a quasi mono-energetic positron beam of $8 \times 10^6/s$. This beam was magnetically guided into a two-stage Surko type trap whose content was dumped into the accumulator four times a second. The accumulator contains a multi-ring potential well in which positrons are stored and manipulated prior to dumping. Each ring is hardwired to an independent external voltage pulser so that the dump may be initiated by applying a parabolic potential along the length of the well. This causes the ejected positrons to arrive at the target at the same time and hence acts as a time focus [10].

Although the accumulator is capable of storing up to 100 million positrons for the present work 5 million per shot was more than sufficient. The

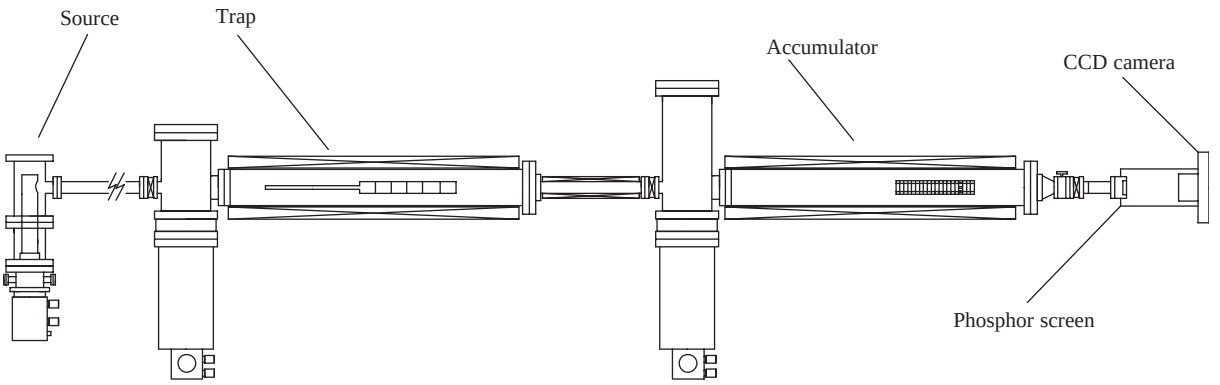

Fig. 1. The layout of the positron accumulator system. A DC positron beam of 8×10^6/s is generated by the solid neon moderator in the source. From this the trap section created pulses containing approximately 250,000 positrons and delivers them to the accumulator at 4 Hz. The accumulator is capable of storing 1×10^8 positrons and can deliver pulses with a spread of approximately 10 ns.

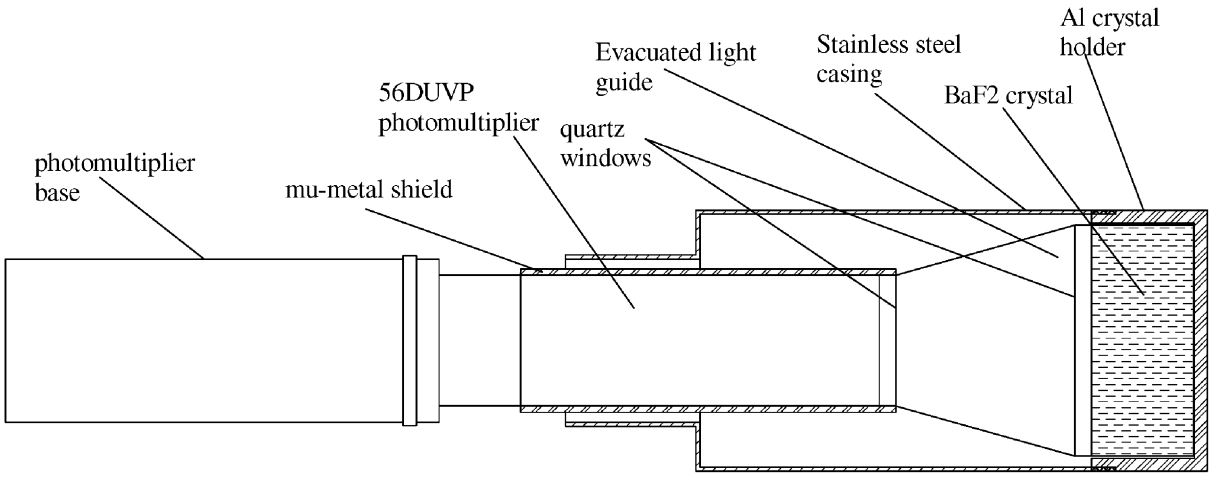

Fig. 2. The design of the BaF_2–PM system adopted in this experiment. Details are described in the text.

positron pulses so obtained were approximately 10 ns FWHM. The BaF_2 crystal used was a 40 mm thick cylinder with diameter $D = 90$ mm. The expected absolute efficiency for the 0.511 MeV photons is $\varepsilon \simeq 95\%$. The scintillator had to be decoupled from the photomultiplier (PM) before it could be heated, to prevent damage to the PM. For this reason, an especially designed detector casing, shown in Fig. 2, was used. BaF_2 is rather sensitive to thermal shocks and so the crystal was housed in an Al holder to help distribute the heat. Thermocouples were placed on the front of the crystal holder and near the cathode of the PM to monitor the heating process. An evacuated glass cone with quartz windows was used as a light guide to thermally insulate the PM from the crystal. The cone was wrapped with Teflon tape to increase the diffuse reflection. A heater tape was used to heat the Al crystal holder and care was taken to keep the temperature gradient at approximately 0.5 °C/min. Air was blown through two holes (not shown in Fig. 2) in the stainless steel casing near the PM and a fan was used externally as an extra precaution. For a crystal temperature of 220 °C the maximum PM temperature was 30 °C.

The PM was operated with negative voltage applied to the photocathode and anode at ground potential. The detector anode was directly coupled to the 50 Ω input of an Agilent Infinium 54855A digital storage oscilloscope which was triggered by the voltage pulser used to initiate the positron dump. Three waveforms were taken at each temperature as the crystal was heated in 20 °C steps. The sampling time was 0.5 ns. Each waveform consisted of 2×10^4 points, spanning a range of 10 μs. The results shown in the next sections are very similar to those obtained with a different setup where two BaF_2 scintillators coupled to XP2020Q PMs and a standard ^{22}Na positron source were employed. In this case the trigger to the temperature controlled scintillator (the same as that shown in Fig. 2) was provided by the anticollinear γ ray reaching the second scintillator, kept at room temperature and coupled directly to the second PM. The main difference between the two experiments was that whereas in the latter system we collected many waveforms to get sufficient statistical precision (each spectrum was averaged over 4096 acquisitions), in the former experiment the information was obtained in one single shot of the positron beam (more precisely, as mentioned above, three shots were employed). Fig. 3 shows a typical waveform of the digital oscilloscope, characterized by a prompt peak followed by a slow decay. Note that the direct study of the anode waveforms adopted in the setting described above has the advantage of reducing the acquisition time to few seconds.

3. Results and discussion

Fig. 4 shows some representative anode time spectra taken at various temperatures. For ease of representation the spectra have been interpolated to a smaller number of points. (In the following, the spectra collected at the various temperatures are denoted as $T40$, $T80$ etc.) Clearly, the trailing edge of the anode signal, attributed to the 300 nm slow component of BaF_2 decreases considerably as a function of temperature. At the highest temperature ($T = 220$ °C), no remnant of the anode decay in the 100–6000 ns region can be observed. On the other hand, the prompt peak of the anode pulse, shown in Fig. 5 at the binning of the original acquisition (0.5 ns/channel), is essentially temperature independent. The FWHM of the prompt peak is $W_T \simeq 12$ ns. This width is consistent with the convolution (approximated by a sum in quadrature) of the intrinsic width of

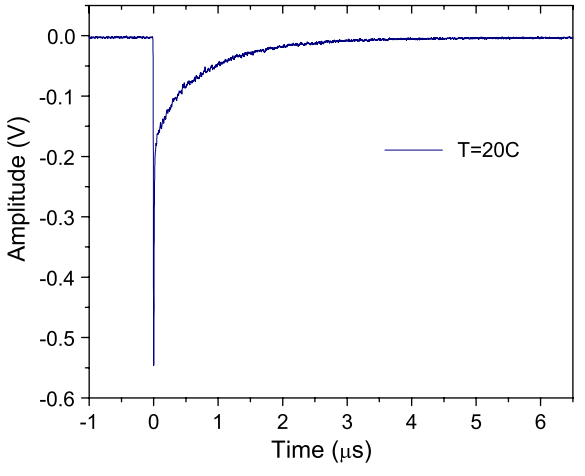

Fig. 3. A typical anode waveform of the digital oscilloscope employed in the data acquisition (at $T = 20$ °C). The 20,000 bins spectrum has been subjected to 15 points smoothing.

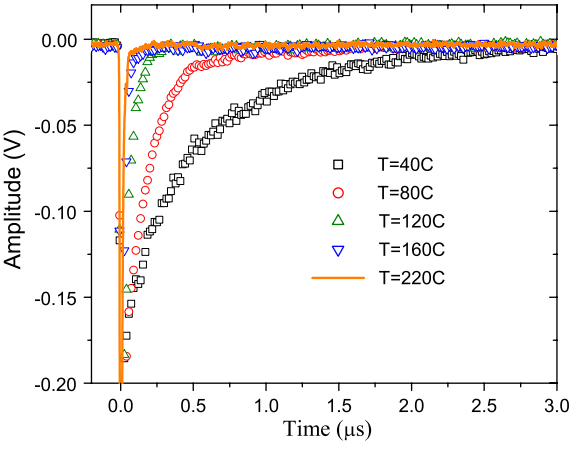

Fig. 4. Some anode traces for various temperatures of the BaF_2 scintillator. The original waveforms have been interpolated into 200 points. The $t = 0$ time coincides with the peak of the prompt. To better visualize the slow decay, the traces have been truncated at amplitudes $V = -0.2$ V.

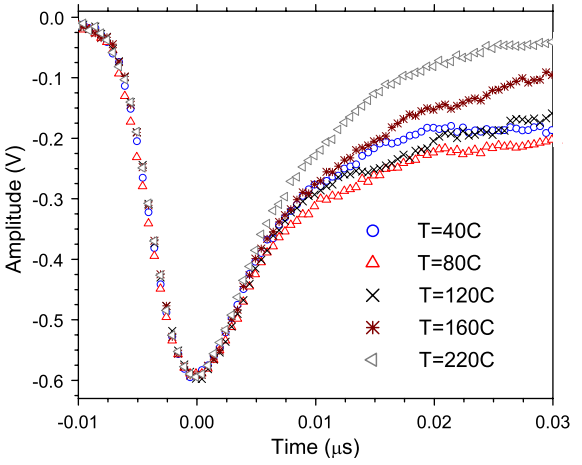

Fig. 5. The same waveforms shown in Fig. 4 near $t = 0$ for the original acquisition binning (0.5 ns/channel).

the PM-scintillator ($W_{PM} \simeq 5$ ns, as measured in separate experiments) with the time spread of the positron pulse ($W_{beam} \simeq 10$ ns, as mentioned above). Note that the FWHM obtained is still sufficiently narrow for future single shot positron lifetime experiments aimed at measuring changes in the lifetime of orthopositronium ($\tau_{vacuum} = 140$ ns) as a function of the positron density, generated by various quenching processes (recall Fig. 1). In these measurements, where up to $\simeq 10^8$ positrons annihilate in a single burst, the overall waveform consists of the superposition of several prompt and slow decays, each caused by the response of the scintillator to a single positronium annihilation. It is therefore clear that the suppression of the slow decay would eliminate a large background in the critical region centred around 100 ns or so where we plan to set a timing window to monitor the changes of the positronium lifetime. Consequently, a large improvement in the sensitivity of our experiments can be predicted with this spectrometer.

A clearer representation of the time shape of the waveforms is provided by plotting them in logarithmic scale after inversion and background subtraction (the background was obtained by the average of the spectra at negative times, for $t < -2\,\mu$s, not shown in Fig. 4). Moreover, to reduce the statistical noise, data have been regrouped into bins having width proportional to the time distance from the prompt peak (located at $t = 0$). The spectra displayed in log scale are rather well approximated by straight lines, addressing the presence of simple exponential decays. To analyse the data more quantitatively we have fitted all spectra as the sum of a fast prompt, to be attributed to the fast decay, followed by a slow decay. Since the time response of the PM is much larger than the fast scintillation [3,11], the prompt peak, $K(t)$, can be viewed essentially as a kernel which mimics the time resolution of the system (i.e. the fast decay is approximated to a delta function). Moreover, the time response of the system is also reflected in the fine features of the slow decay. The fitting function $f(t)$ adopted is, therefore,

$$f(t) = A\ K(t) + K(t) \oplus B\ D(\lambda, t) \tag{1}$$

where the symbol $\oplus$ denotes the convolution operator, $D(\lambda, t)$ is a sum of exponentials with time decays λ and A, B, λ are fitting parameters. The unknown kernel $K(t)$ is approximated by the $T220$ spectrum [12]. The fitting procedure confirmed that the spectra are well approximated by employing a single exponential decay in $D(\lambda, t)$ [13]. Fig. 6 shows the good agreement between

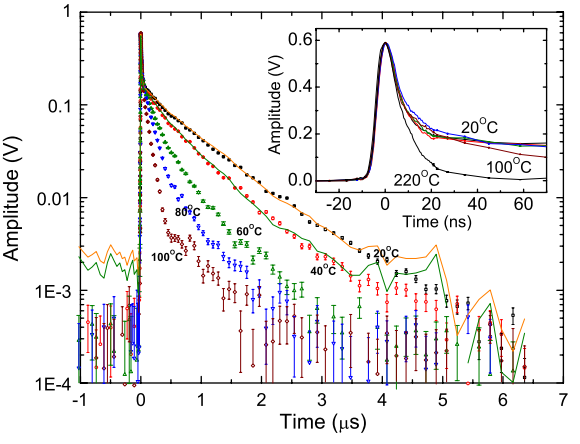

Fig. 6. Selected anode traces for various temperatures, after background subtraction, invertion and rebinning as described in the text. The inset shows the prompt peak of the same spectra. In the main graph, the continuous lines superimposed onto the $T20$ and $T40$ spectra are obtained from the fit described in the text.

waveforms $T20$, $T40$ as examples and the corresponding fits with a single exponential decay. Note that the noise present in the fitted curves is due to the convolution of a pure exponential with the experimental (i.e. noisy) kernel spectrum. A representative example of the agreement between data and model on a magnified time scale near to $t = 0$ is shown in Fig. 7 for the $T40$ spectrum. It can be observed that the good agreement between data and model persists to a large extent at the merging between prompt peak and longer decay (at $t \simeq 15$ ns).

The lifetimes of the slow component (τ_S) and the intensities of slow and fast component (I_S, I_F) as a function of the acquisition temperature are shown in Fig. 8A. Whereas I_S decreases drastically with temperature, I_F is constant. To facilitate the comparison with previous studies, the intensities have been renormalized to number of photons/keV, employing the room temperature photon/keV yield for the slow decay reported in Ref. [1]. Fig. 8B shows the relative intensities of I_S and I_F in percent. The values of τ_S and I_S [(0.66 ± 0.02)μs, (89 ± 2)%] at room temperature are in good agreement with the average results quoted in Refs. [3,7], although both papers claim to separate two components in the slow decay. We can conjecture that the level of precision of the data acquisition (particularly at $t > 4$ μs) is such that we are unable to resolve the two components in the fit. In any case, as discussed above, in our analysis the slight departures from a single decay behaviour can be accounted by the inclusion of the kernel $K(t)$ in the fitting procedure (see Ref. [13]).

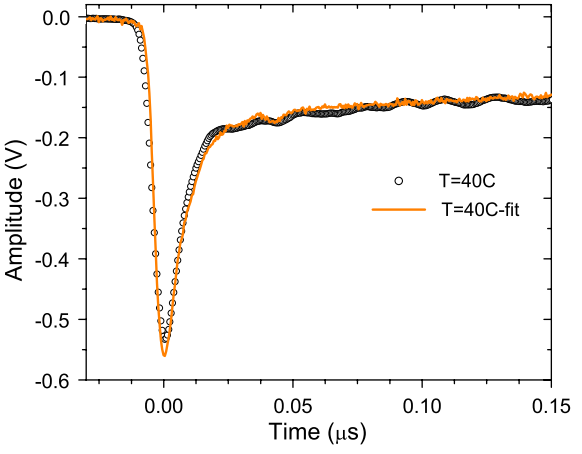

Fig. 7. The $T40$ spectrum and the fitting function described in the text in the $[-25, 150]$ ns time interval.

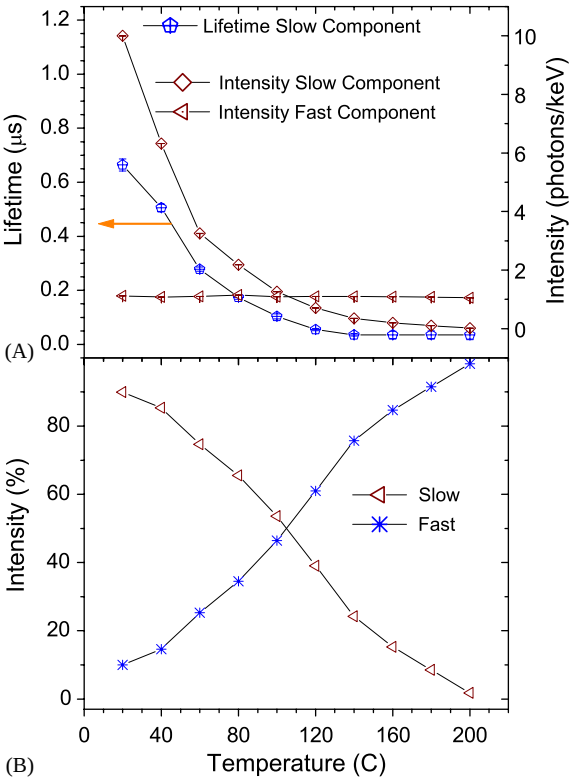

Fig. 8. (A) The lifetime of the long components of BaF_2 and the absolute intensities of the fast and slow components as a function of temperature. The intensities have been rescaled in terms of number of photons/keV, according to the room temperature photon yield for the slow decay reported in Ref. [1]. (B) The relative intensities of the two components, in percent. In both plots the continuous lines are merely guides to the eye.

The origin of the slow and fast decays in BaF_2 has been discussed extensively [14–17]. There is a consensus in ascribing the fast decay to the transition of electrons from a $2pF^-$ band to the hole caused in the $2pBa^{2+}$ band by the electron excitation due to the irradiation. This decay, observed in the luminescence spectra as peaks at 190 and 220 nm, has been denoted by a variety of

short-cut definitions such as *crossover transition* (CT) [14,15], *core to valence photoluminescence* (CVL) [16], or *Auger electron free luminescence* [17]. Nevertheless, all authors agree on the electronic transition mentioned above (from $2pF^{-}$ to $2pBa^{3+}$).

On the other hand, the slow decay is ascribed to the radiative decay of the so called (electron-hole) *self-trapped exciton* (STE). Since all the theories [16,15] propose that the STE is a shallow trap, it is natural to assume that it can be quenched by thermal phonons. Consequently, from our temperature dependent data, we can address the question of the apparent binding energy of the STE. From the simple one-trap model we know that a trap can modify a rising or a decaying part of the scintillation time profiles introducing a characteristic non-radiative decay rate [18]

$$\lambda_{nr} = G\exp\left(-\frac{E}{k_B T}\right) \tag{2}$$

where G and E are the frequency factor and trap depth, respectively. At a given temperature, the decay rate of the slow component observed (λ_S) is $\lambda_S = \lambda_r + \lambda_{nr}$ where λ_r and λ_{nr} are the radiative decay rate and the rate at which the STE decays non-radiatively, due to thermal quenching. The observed decay rate can then be fitted as

$$\lambda_S = \lambda_r + G\exp\left(-\frac{E}{k_B T}\right). \tag{3}$$

Fig. 9 shows the result of the fit. To test the consistency of our measurements with previous ones, in Fig. 9 the inverse of the lifetime values measured in Ref. [7] at 0 °C, −25 °C and −45 °C, have been included and fitted with the same model (Eq. (3)). The lowest temperature additional points are well described by the model, yielding an overall binding energy of the STE, $E = (0.25 \pm 0.01)\,\mathrm{eV}$ [19]. Conversely, the fit cannot account of the apparent saturation of the lifetimes at high temperature. In this regard, one should realize that the closer the spectra are to the $T220$ waveform, assumed as kernel $K(t)$, the smaller is the significance of the lifetime values yielded by the fitting procedure of Eq. (1) (and the larger are the uncertainties). On the other hand, the intrinsic decay rate, $\lambda_r = 0.15 \times 10^6/\mathrm{s}$ yields a lifetime $\tau_S = (6.7 \pm 0.4)\,\mu\mathrm{s}$, which is consistent with the results of Ref. [7].

Finally (Fig. 10), we account for the time dependence of the absolute intensity, $I_S(T)$ assuming

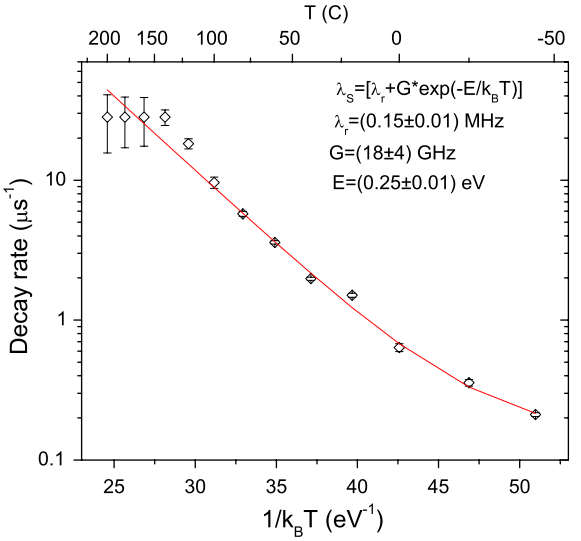

Fig. 9. The decay rate of the slow component, fitted with the function described in the text and shown in the figure. The three lower temperature points (corresponding to $T = 0$, -25, -45 °C) have been derived from Fig. 3(b) in Ref. [7].

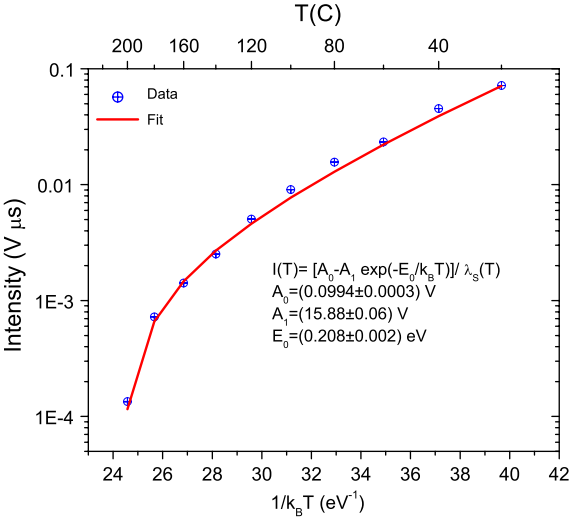

Fig. 10. The intensity of the slow component, plot in log scale vs $1/k_B T(K)$, fitted with the function described in the text and shown in the figure. The errors are smaller than the sizes of the dots.

a temperature dependence amplitude of the decay, $A(T)$

$$A(T) = A_0 - A_1 \exp\left(-\frac{E_0}{k_B T}\right). \quad (4)$$

Consequently,

$$I_S(T) = \frac{A(T)}{\lambda_S(T)} \quad (5)$$

where $\lambda_S(T)$ is given by Eq. (3). The decrease in the amplitude addresses the possibility that other thermal processes reduce the probability of formation of the STE (described by the coefficient A_1). In the fit of the intensity we have let A_0, A_1 and E_0 be free parameters, and fixed the parameters for $\lambda(T)$ to the values obtained previously. The value of $E_0 = (0.208 \pm 0.002)$ eV is lower than the value obtained fitting the lifetime. This is not very surprising, since the number of STE's which form is mostly conditioned by density and diffusion of electrons and holes, whereas the number of STE's thermally quenched is uniquely affected by the density of phonons.

4. Conclusions

In this work we have sketched a procedure to study the decay of the luminescence in scintillators. The method, greatly facilitated by the enormous improvement in the state of the art digital oscilloscopes in terms of sampling frequency and data acquisition, consists in the direct analysis of the anode output of the scintillator–PM system, suitably triggered. This technique has been employed to study the thermal quenching of the slow decay of the BaF_2 scintillator. The quenching is essentially complete at a temperature $T_Q \simeq 200\,^{\circ}C$. From the temperature dependence of the single lifetime of the slow decay τ_S we estimate the binding energy of the self-trapped exciton responsible of the transition to be $E = (0.25 \pm 0.01)$ eV. It is also worth emphasizing that the adoption of a BaF_2-based detector where the slow component is suppressed should improve noticeably the precision of single shot lifetime experiments in the typical range of the orthopositronium lifetime (50–150 ns), which are planned for the pulsed beam, consisting of bursts of $\simeq 10^8$ positrons, described in this work.

Acknowledgements

We are grateful to Rod Greaves of First Point Scientific for valuable comments and advice and Brian Williams for help with instrumentation. This work was supported in part by the JSPS core to core program, the National Science Foundation under grants PHY-0140382 and DMR-0216927 and by DOD/DARPA/DMEA under Award no. DMEA90-02-2-0216.

References

[1] E.g., S. Derenzo, W.W. Moses, M.J. Weber, A.C. West, Proceedings of the Material Research Society: Scintillator and Phosphor Materials, vol. 348, 1994, p. 39.
[2] R.N. West, Positron in solids, in: P. Hautojarvi (Ed.), Topics in Current Physics, Springer, Berlin, 1979, p. 89.
[3] M. Laval, M. Moszynski, R. Allemand, E. Comoreche, P. Guinet, R. Odru, J. Vacher, Nucl. Instr. and Meth. 206 (1983) 169.
[4] For "fast" a useful metric is the typical single electron response time of the photomultiplier to be used. This is usually of the order of a few ns, although single stage channel plate multipliers can be as fast as 220 ps (FWHM).
[5] P.J. Simpson, R. Tjossem, A.W. Hunt, K.G. Lynn, V. Munn, Nucl. Instr. and Meth. Phys. Res. A 505 (2003) 82.
[6] P. Schotanus, C.W.E. Van Ejik, R.W. Hollander, J. Pijpelnik, Nucl. Instr. and Meth. A 238 564.
[7] V. Nanal, B.B. Beck, D.J. Hofman, Nucl. Instr. and Meth. A 389 (1997) 430.
[8] L.M. Bollinger, G. Thomas, Rev. Sci. Instrum. 32 (1961) 1044.
[9] R.G. Greaves, J. Moxom, in: M. Schauer et al. (Eds.), Non-Neutral Plasma Physics V, AIP Conf. Proc. 692 (2003) 140.
[10] W.S. Crane, A.P. Mills Jr., Rev. Sci. Instrum. 56 (1985) 1723.
[11] Whereas the time decay of the fast component is about 600 ps, the leading edge, trailing edge and FWHM of the PM Philips 56DUVP are 2, 3 and 5 ns, respectively.
[12] The fitting procedure of the 20,000 channels spectra, based on the standard gradient-expansion algorithm of Marquardt, was considerably sped up by applying the well-known convolution theorem, stating that $K \oplus D = FT^{-1}[FT(K)\ FT(D)]$, where FT is the (fast) Fourier transform. Note that in the fit of the oscilloscope waveform all channels were equally weighted.

[13] The replacement of one exponential with the sum of two in the theoretical function $D(\lambda, t)$ did not lead to any improvement of the reduced CHI square which, actually, got slightly worse (about 0.01%). Indeed, the fit with two exponentials would appear completely superimposed onto the fit with one exponential in the log scale summary shown in Fig. 6.
[14] Ya.A. Valbis, Z.A. Ranchko, Ya.L. Yansons, JETP Lett. 42 (1985) 172.
[15] R. Visser, P. Dorenbos, C.W. van Eijk, H.W. den Hartog, J. Phys.: Condens. Matter 4 (1992) 8801.
[16] A.J. Wojtowicz, P. Szupryczynski, J. Glodo, W. Drozdowski, D. Wisniewski, J. Phys.: Condens. Matter 12 (2000) 4097.
[17] K. Kimura, J. of Electron Spectrosco. Relat. Phenom. 79 (1996) 43.
[18] A.J. Wojtowicz, J. Glodo, D. Wisniewski, A. Lempicki, J. Lumin. 72–74 (1997) 731.
[19] By neglecting the three additional low temperature points, the resulting binding energy of the STE is $E = (0.30 \pm 0.02)$ eV, consistent with the fact that the log of decay rate vs $1/k_B T$ is steeper at higher temperature (see Fig. 9).